

Cite this article as: Wan Xuan, He Chaowei, Zhang Kezhao, et al. Influence of Aging Treatment on Microstructure and Properties of Ti-3Al-6Mo-2Fe-2Zr Laser-Welded Joint[J]. Rare Metal Materials and Engineering, 2025, 54(04): 930-936. DOI: <https://doi.org/10.12442/j.issn.1002-185X.20240109>.

ARTICLE

Influence of Aging Treatment on Microstructure and Properties of Ti-3Al-6Mo-2Fe-2Zr Laser-Welded Joint

Wan Xuan, He Chaowei, Zhang Kezhao, Liu Dong, Yan Chunyan, Bao Yefeng

College of Materials Science and Engineering, Hohai University, Changzhou 213022, China

Abstract: Laser beam welding was used to join a near- β titanium alloy (Ti-3Al-6Mo-2Fe-2Zr), followed by aging treatments. The relations among aging temperature, microstructure, and tensile properties of joints were revealed. For as-welded joints, the fusion zone features primarily single β phase. It is attributed to the high Mo equivalency of this alloy and the fast cooling rate in laser beam welding. After aging treatments, many α precipitates form in the fusion zone and heat affected zone. The rising aging temperature coarsens α precipitates and reduces the volume fraction of α precipitates. Compared with the as-welded joints, the aging treated joints' tensile strength and elongation are improved. The increasing aging temperature weakens the strengthening effect because of the decreasing volume fraction of α precipitates. After the aging treatment at 500 °C for 8 h, the joints obtain the optimal match between strength and plasticity. The fracture mode of joints changes from quasi-cleavage fracture in as-welded condition to microvoid coalescence fracture after heat treatments.

Key words: β titanium alloy; laser beam welding; heat treatment; microstructure evolution; room temperature tensile property

1 Introduction

Given their excellent hardenability, superior corrosion resistance capability, and high strength-to-weight ratio, β titanium alloys have obtained significant attention in aerospace industry and marine engineering. β titanium alloys belong to a type of titanium alloy, whose tensile strength and plasticity can be adjusted over a wide range by modifying the α phase's size, volume fraction, and morphology through heat treatment^[1]. Compared to other titanium alloys, β titanium alloys offer a better balance between strength and plasticity.

The efficient and reliable welding process is crucial for the applications of titanium alloys. Laser beam welding is widely recognized for its low heat input, high efficiency, and adaptability to both thin and thick plates. Extensive research has been conducted on the laser weldability of different β titanium alloys. These studies have revealed that the fusion zone mainly consists of β phase in as-welded condition^[2-4]. This is because of the existence of a significant amount of β -stabilizing elements and the fast cooling rate in the laser

welding process, which promotes the formation of β phase. As a consequence of the absence of strengthening phase, the tensile properties of the joints are lower after laser beam welding. Therefore, post-weld heat treatment (PWHT) is necessary to improve the strength of laser-welded β titanium alloys. Lei et al^[5] studied the influence of PWHT on TB8 joints by laser-oscillated welding. The as-welded fusion zone was composed of single β phase in as-welded condition. After low temperature aging (350–450 °C), the microstructure of joint consists of ω and β phases. In contrast, the high-temperature aging (500–600 °C) results in fusion zone consisting of α and β phases. Lei's findings demonstrated that the tensile properties can be improved by proper aging treatment. Long et al^[6] investigated the influence of PWHT on laser-welded Ti-55531 (Ti-5Al-5V-5Mo-3Cr-1Zr) joints. The outcomes further confirmed that the fusion zone in the as-welded joints consists entirely of β phase. After PWHT, numerous acicular α phases are produced in the fusion zone. As a result, the tensile strength and microhardness are improved by the precipitation of α phase.

Received date: April 01, 2024

Foundation item: National Natural Science Foundation of China (51804097); Fundamental Research Funds for the Central Universities of China (B220202026); Changzhou Sci&Tech Program (CJ20220074)

Corresponding author: Zhang Kezhao, Ph. D., Associate Professor, College of Materials Science and Engineering, Hohai University, Changzhou 213022, P. R. China, E-mail: zhangkz@hhu.edu.cn

Copyright © 2025, Northwest Institute for Nonferrous Metal Research. Published by Science Press. All rights reserved.

Herein, the laser beam welding was used to join a near- β titanium alloy (Ti-3Al-6Mo-2Fe-2Zr, wt%). Aging treatments at different temperatures were applied to the laser-welded joints. The relationships among aging temperature, microstructure, and tensile property of joints were discussed. The constituent phases formed under different aging conditions were analyzed. The morphology, size, and volume fraction of strengthening phase were also studied. The findings of this research provide valuable guidance for the aging treatment of laser-welded Ti-3Al-6Mo-2Fe-2Zr joints.

2 Experiment

Ti-3Al-6Mo-2Fe-2Zr (wt%) plates with 2 mm in thickness were adopted for the laser welding process, whose chemical composition is listed in Table 1. Fig. 1 illustrates the phase composition of base metal. As can be seen, two different α phases are dispersed uniformly in β matrix. The ellipsoidal α is identified as primary α (α_p) phase, and the acicular α is identified as secondary α (α_s) phase. The size of α_s phase is much smaller than that of α_p phase.

The $[\text{Mo}]_{\text{eq}}$ (Mo equivalency) is usually used to distinguish different β titanium alloys^[7]. The Mo equivalency of near- β titanium alloy is 8.5%–13.8%. In this research, $[\text{Mo}]_{\text{eq}}$ of the used alloy is 13.49%, which is calculated by Eq. (1) and listed in Table 1, indicating that this alloy belongs to a near- β titanium alloy. The elements in Eq. (1) are expressed in mass percentage (wt%).

$$[\text{Mo}]_{\text{eq}} = \text{Mo} + \frac{\text{Fe}}{0.5} + \frac{\text{W}}{2} + \frac{\text{Ni}}{0.8} + \frac{\text{Cr}}{0.6} + \frac{\text{Mn}}{0.6} + \frac{\text{V}}{1.4} + \frac{\text{Co}}{0.9} + \frac{\text{Nb}}{3.3} + \frac{\text{Ta}}{4} \quad (1)$$

The power of laser beam was set to 1200 W, and the speed was set to 1.0 m/min. The parameters for the aging treatments are presented in Table 2. The aging temperature was set to be much lower than the equilibrium transition temperature of $\alpha \rightarrow \beta$ phase transformation. The reason is that higher aging temperature can promote the $\alpha_p \rightarrow \beta$ transformation, which weakens the pinning effect of α_p phase and leads to the

Table 1 Chemical composition of Ti-3Al-6Mo-2Fe-2Zr alloy (wt%)

Ti	Al	Fe	Zr	Mo
83.97	3.31	2.89	2.21	7.71

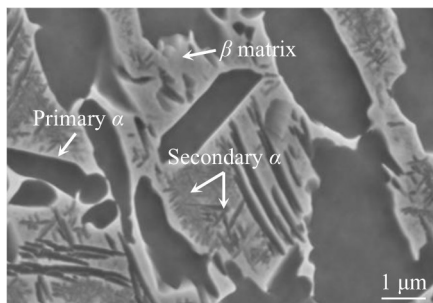


Fig. 1 Microstructure of base metal

Table 2 Parameters for aging treatments

No.	Aging temperature/°C	Aging time/h
1	400	8
2	500	8
3	600	8

coarsening of β grains. To prevent oxidation during aging process, the samples were placed in a vacuum quartz tube prior to aging treatment.

The metallographic samples were sequentially polished and etched for microstructural analysis. The Kroll's reagent, composed of 5% hydrogen fluoride, 35% hydrogen nitrate, and 60% deionized water, was used for the etching process. The microstructures of the cross-section of joints were observed by scanning electron microscope (SEM, ZEISS Gemini SEM 300 and JSM-7800). Further microstructural analysis of the fusion zone was performed by the transmission electron microscope (TEM). Samples for TEM analysis were selected from the center of fusion zone and polished to the ones with thickness of 30–40 μm . The elements distribution in fusion zone was analyzed using TEM equipped with energy disperse spectroscopy (EDS). The tensile properties were evaluated by an electronic universal tensile testing machine (UTM 5015). Afterwards, the fracture surface was observed by SEM (ZEISS Gemini SEM 300).

3 Results and Discussion

3.1 As-welded joints

Fig. 2 presents the optical microscopic image of as-welded joints. The microstructure of fusion zone features entirely β columnar grains with relatively large size. The dendrites are observed within β columnar grains. Due to the high energy density of laser welding, there is a significant temperature difference between the center and the edge of the fusion zone, which directly results in the large temperature gradient in liquid metal. Therefore, the β grains grow into columnar crystals from fusion line to fusion zone center along the orientation of the largest temperature gradient. Meanwhile, the compositional undercooling induced by the redistribution of solute elements can promote the generation and growth of dendrites in the rapid cooling process.

The fusion zone in as-welded condition was examined

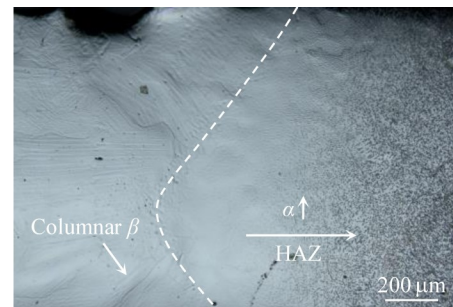


Fig. 2 Optical microscopic image of as-welded joints

using TEM, as shown in Fig.3. From bright field (BF) image, there are no secondary phases in β matrix. Additionally, the selected area electronical diffraction (SAED) pattern of fusion zone also proves the aforementioned result, revealing the presence of β phase with body-centered cubic (bcc) structure in the fusion zone. During the heating stage of laser welding process, the $\alpha_p/\alpha_s \rightarrow \beta \rightarrow$ liquid metal transformations proceed in base metal in turn, and the molten pool is formed correspondingly.

As the laser welding process goes on, the molten pool will experience the extremely fast cooling process. The high content of β -stabilizing elements ($[\text{Mo}]_{\text{eq}}=13.49\%$) and the fast cooling rate in fusion zone can completely suppress the $\beta \rightarrow \alpha$ transformation^[8], thereby leading to the absence of α phase in β matrix.

Fig. 4 displays the microstructure of heat affected zone (HAZ). Based on the microstructure features, three areas in HAZ are verified with increasing the distance to fusion zone. The area composed of single β phase is identified as near-HAZ (Fig.4a). The areas consisting of β +retained α_p and β + α_p +retained α_s are identified as mid-HAZ (Fig.4b) and far-HAZ (Fig.4c), respectively. The varied thermal cycles experienced in different regions during the laser welding process are responsible for the diverse microstructures in the HAZ. In the near-HAZ, which is the closest region to the fusion zone, the peak temperature during the heating process is higher than the equilibrium transition temperature of $\alpha \rightarrow \beta$ transformation. As a result, a complete $\alpha \rightarrow \beta$ transformation occurs in this region. In the subsequent cooling process, the high $[\text{Mo}]_{\text{eq}}$ and the fast cooling rate help to keep the primary and transformed β phases to ambient temperature. Nevertheless, in the thermal

cycle of mid-HAZ, the peak temperature is close to the equilibrium transition temperature of $\alpha \rightarrow \beta$ transformation, which is difficult to promote the thorough $\alpha \rightarrow \beta$ transformation. Some of the primary α_p phase in this region remain to ambient temperature. In the far-HAZ, the peak temperature and duration of high temperature decrease further, which is unfavorable for the $\alpha \rightarrow \beta$ transformation. The $\alpha_p \rightarrow \beta$ transformation requires longer holding time than the $\alpha_s \rightarrow \beta$ transformation. Hence, a majority of ellipsoidal α_p and acicular α_s with comparatively larger size remain in far-HAZ.

3.2 Influence of aging temperature on microstructure

The optical microscopic and SEM images of the joints at different aging temperatures are displayed in Fig.5. After the aging treatments, massive precipitates form in fusion zone and HAZ, especially in the near-HAZ which is composed solely of β phase in as-welded condition. As the aging temperature increases, the size of precipitates increases, as characterized in Fig.5d–5f. Besides, the aging treatment has no influence on the morphology and size of β columnar grains in fusion zone and near-HAZ.

Fig.6 presents the optical microscopic and SEM images of fusion zone at different aging temperatures. After aging treatment, many precipitates form within β columnar grains, as illustrated in Fig.6a, 6d and 6g. The size and volume fraction of precipitates are closely related to the aging temperature in the fusion zone. At 400 °C (Fig.6c), the morphology of precipitates cannot be recognized clearly because of the fine size. At 500 and 600 °C (Fig.6f and 6i), the needle-like precipitates are distributed homogeneously in β matrix. Meanwhile, the rising aging temperature coarsens the precipitates and declines the volume fraction of precipitates.

Fig.7 and Fig.8 present the TEM images of the fusion zone at different aging temperatures. Fig.7 shows the microstructure characteristic of fusion zone at 400 °C. In the SAED pattern along the zone axis of $[110]_\beta$ (Fig.7a), the diffraction spots of β (marked by white arrow), ω (marked by red arrow), and α (marked by yellow arrow) phases are observed, indicating that the constituent phases of precipitates at 400 °C are β , ω , and α phases. The diffraction pattern of ω phase is much weaker than that of α phase. It can be inferred that the proportion of ω phase is much lower than that of the α precipitates. The corresponding BF image indicates that the α precipitate has needle-like morphology with length of 31–47 nm. The high resolution TEM (HRTEM) image along the

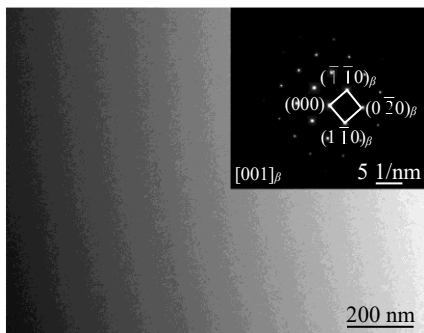


Fig.3 TEM image of fusion zone in as-welded condition

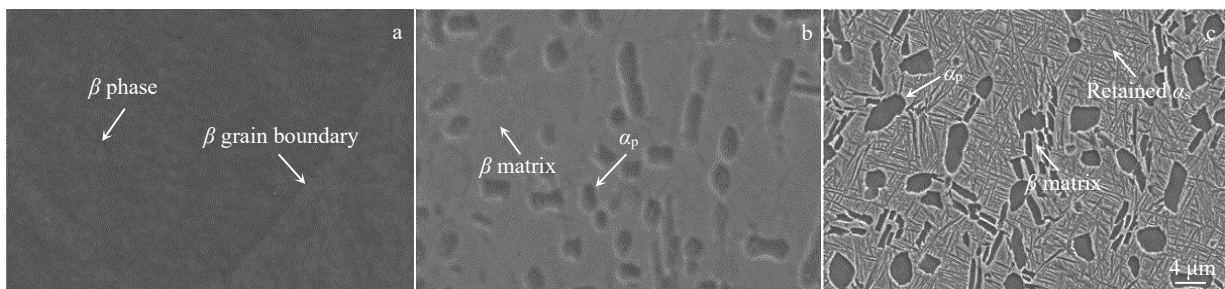


Fig.4 Microstructures of HAZ of as-welded joint: (a) near-HAZ, (b) mid-HAZ, and (c) far-HAZ

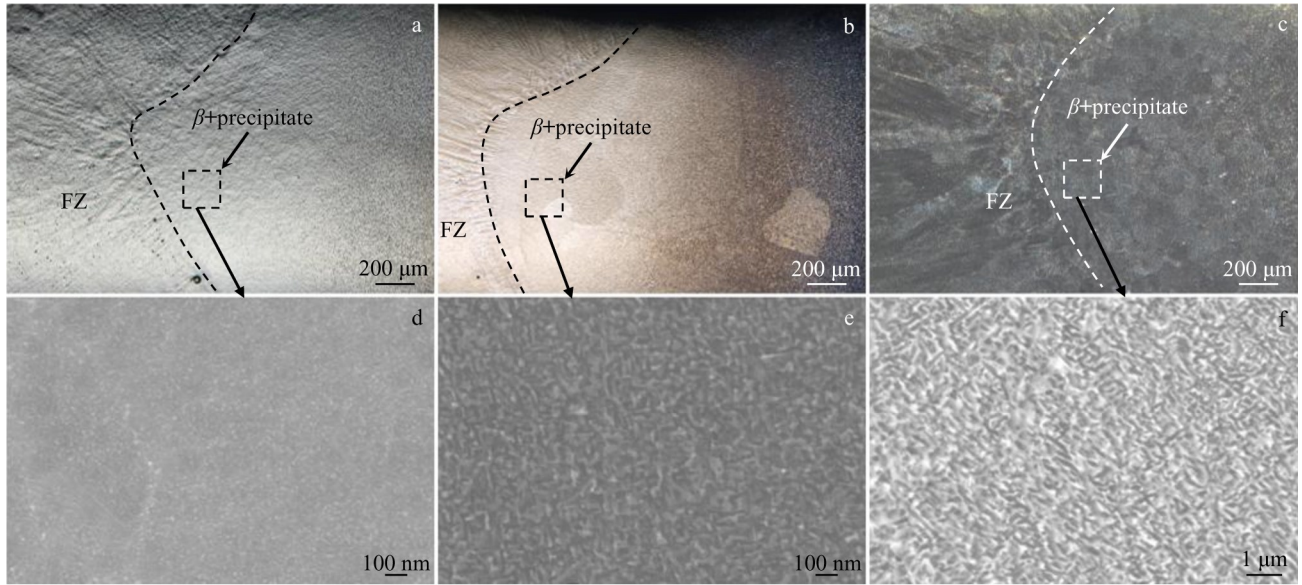


Fig.5 Microstructures of joints at different aging temperatures: (a–d) 400 °C, (b–e) 500 °C, (c–f) 600 °C (FZ: fusion zone)

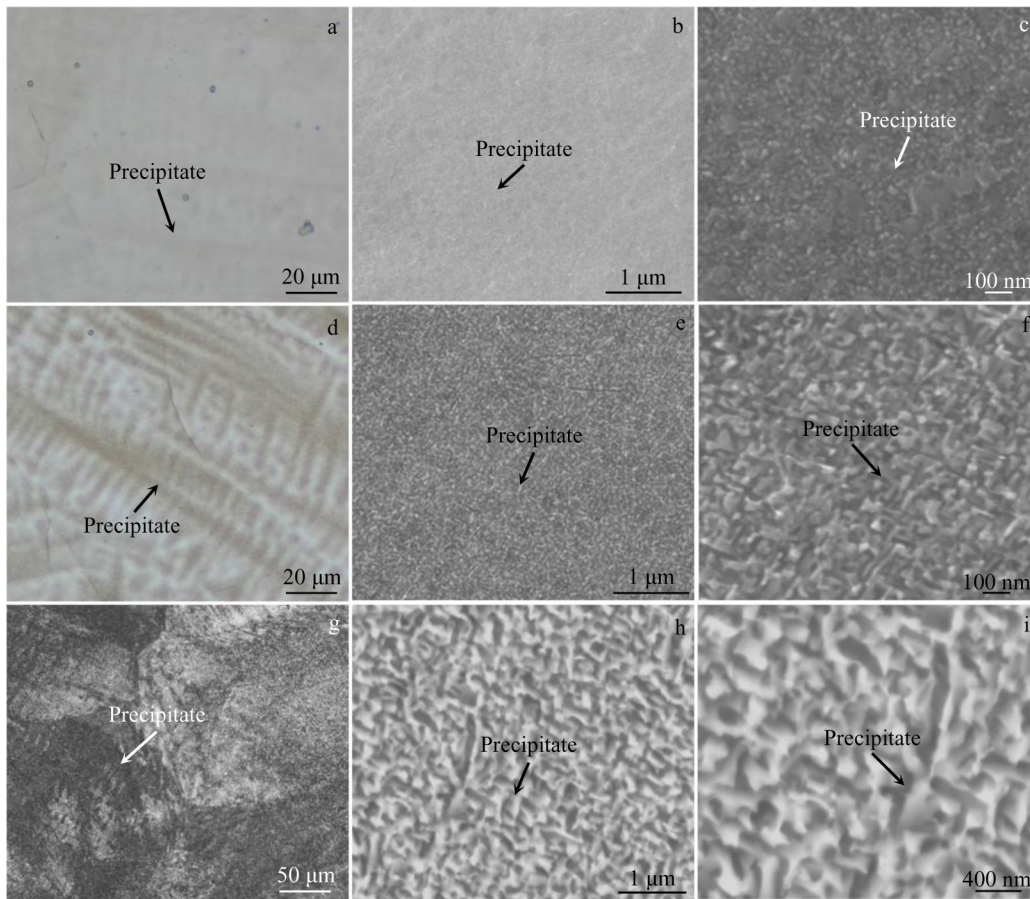


Fig.6 Microstructures of fusion zone at different aging temperatures: (a–c) 400 °C, (d–f) 500 °C, and (g–i) 600 °C

zone axis of $[110]_{\beta}$ is adopted to analyze the lattice transition and orientation relationships among β , ω , and α phases in the fusion zone at 400 °C, as illustrated in Fig. 7b – 7c. The hexagonal close-packed (hcp) α precipitate and hexagonal non-close-packed (hnpc) ω precipitate are verified in bcc β

matrix (Fig. 7b), which is consistent with Fig. 7a. In order to further analyze the relationship between precipitates and β matrix, the fast Fourier transform (FFT) was carried out on the blue square area in Fig. 7b, as displayed in Fig. 7c, in which the diffraction spots of β , α , and ω phases are observed.

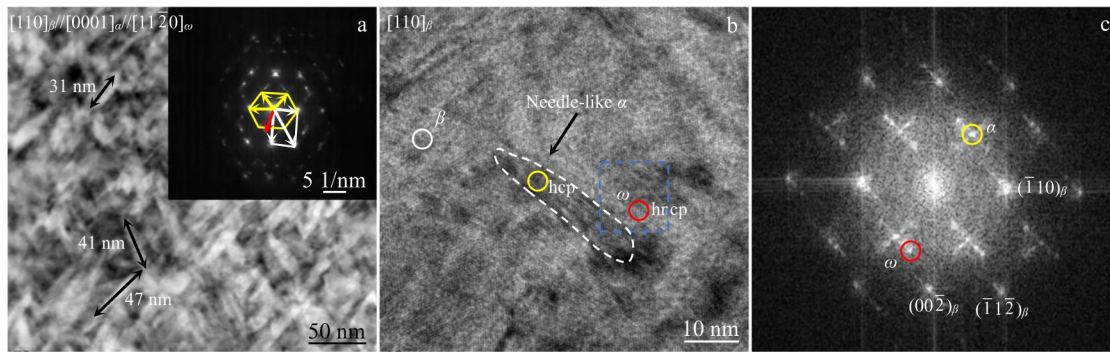


Fig.7 TEM images of fusion zone at aging temperature of 400 °C: (a) BF TEM image and SAED pattern along $[110]_{\omega}//[0001]_{\alpha}//[11\bar{2}0]_{\omega}$ zone axis, (b) HRTEM image along $[110]_{\beta}$ zone axis, and (c) FFT image of region marked by blue square in Fig.7b

Fig. 8 displays the microstructural characteristic of fusion zone at 500 and 600 °C. At 500 °C (Fig. 8a), the precipitate in β matrix is identified to be hcp α phase, of which the length is 73–113 nm. No ω phase is observed in β matrix. At 600 °C (Fig.8b), the length of needle-like α rises to 555–727 nm, and the volume fraction decreases significantly.

The phase transformation process changes with the aging temperature. Previous research has demonstrated that for β titanium alloys, the $\beta \rightarrow \omega$ transformation starts at 300 °C. As the aging temperature reaches 400 °C, the $\beta \rightarrow \omega \rightarrow \alpha$ transformation occurs in turn, with the ω phase as transition phase. At 500 °C and higher aging temperatures, the α phase is more likely to precipitate directly from β matrix^[9]. The formation of needle-shaped α precipitates at 400 °C is closely related to the ω -assisted nucleation. It is demonstrated that the transformation mechanism of isothermal ω phase is attributed to the collapse of atomic layer and element diffusion in β titanium alloys^[10]. During the aging treatment, ω -destabilizing elements (Mo, Al) within ω phase gradually diffuse into the surrounding region of ω phase, resulting in the enrichment of Al element at ω/β interface. As the aging treatment progresses, α phase will nucleate at ω/β interface containing lots of α -stabilizing elements and grow by a displacive-diffusive mixed mechanism. Meanwhile, ω phase is replaced by α phase gradually. At 500 and 600 °C, the α phase is more likely to precipitate directly from β matrix. During the aging treatment at 500 and 600 °C, Al element diffuses into the Mo-lean region, as displayed by high-angle annular dark-field (HAADF) image in Fig.9. As the diffusion process progresses, the concentration of Al element in Mo-lean region gradually increases, which further contributes to the nucleation and growth of α phase in this area. Consequently, the dual-phase microstructure composed of β phase and needle-shaped α phase is formed after the aging treatments at 500 and 600 °C. The decrease in the proportion and increase in the size of α phase with rising aging temperature can be explained by the nucleation rate and atomic diffusion. As the aging temperature rises, the driving force for α nucleation diminishes, resulting in a reduction in number of α nuclei and, consequently, a decrease in volume fraction. Meanwhile, the increment of aging temperature increases the atomic diffusion rate, which facilitates the rapid growth of α nucleus.

As the diffusion process progresses, the concentration of Al element in Mo-lean region gradually increases, which further contributes to the nucleation and growth of α phase in this area. Consequently, the dual-phase microstructure composed of β phase and needle-shaped α phase is formed after the aging treatments at 500 and 600 °C. The decrease in the proportion and increase in the size of α phase with rising aging temperature can be explained by the nucleation rate and atomic diffusion. As the aging temperature rises, the driving force for α nucleation diminishes, resulting in a reduction in number of α nuclei and, consequently, a decrease in volume fraction. Meanwhile, the increment of aging temperature increases the atomic diffusion rate, which facilitates the rapid growth of α nucleus.

3.3 Tensile properties

The tensile properties of laser-welded joints in as-welded and heat-treated conditions are exhibited in Fig.10. As can be found, after the aging treatment, the tensile properties of joints are improved prominently. The ultimate tensile strength (UTS) of joints is reduced gradually and the elongation rises with increasing the aging temperature. The joints aged at 500 °C for 8 h achieve the optimal balance between strength and plasticity.

The tensile properties are closely associated with the microstructural characteristics of joints. In the as-welded condition, the microstructure of fusion zone and near-HAZ primarily consists of β phase. In titanium alloys, the α phase

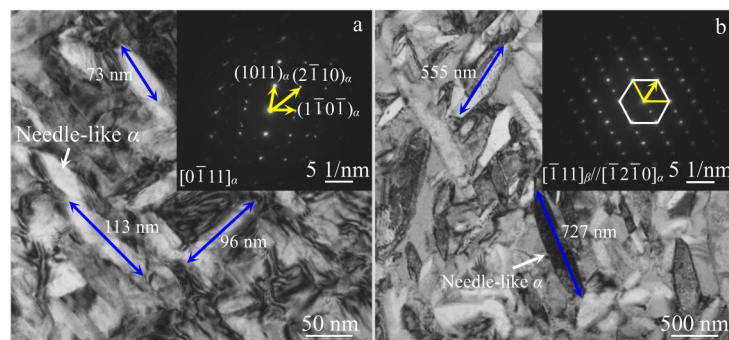


Fig.8 BF TEM images and SAED patterns of fusion zone at aging temperature of 500 °C (a) and 600 °C (b)

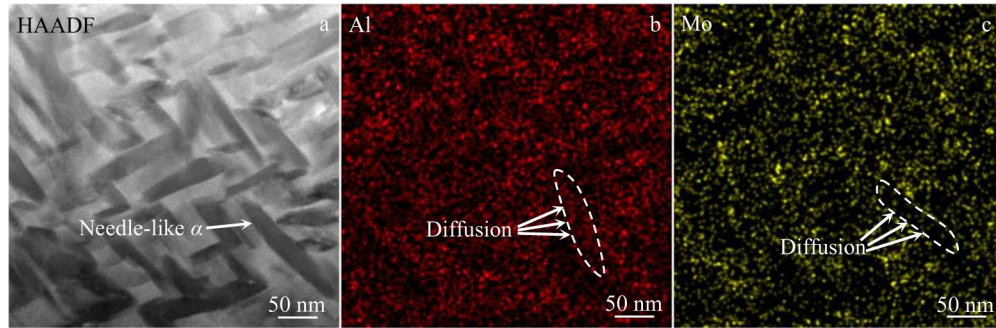


Fig.9 HAADF of fusion zone after aging treatment at 500 °C (a); corresponding EDS mappings of element Al (b) and Mo (c)

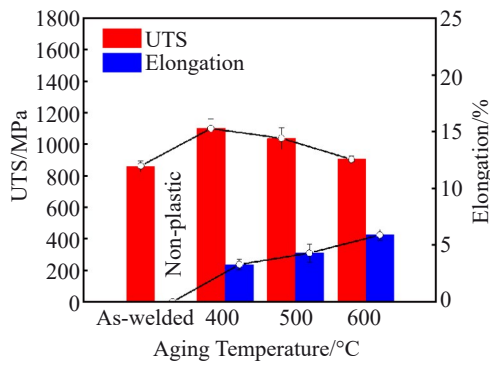


Fig.10 Influence of aging treatment on tensile properties of joints

usually works as a strengthening phase because of its higher deformation resistance compared with the β phase. Meanwhile, the α/β boundaries can hinder dislocation movement due to the lattice misfit between α and β phase^[11]. Without the strengthening effects of α phase, the strength of joints is relatively lower in as-welded condition. As the aging temperature increases, the length of needle-like α grows (from 31–47 nm at 400 °C to 555–727 nm at 600 °C), and the volume fraction decreases accordingly. Previous research has proved that a smaller size and higher volume fraction of α phase generally lead to a stronger second-phase strengthening effect, on account of more α/β interfaces^[12]. A high density of

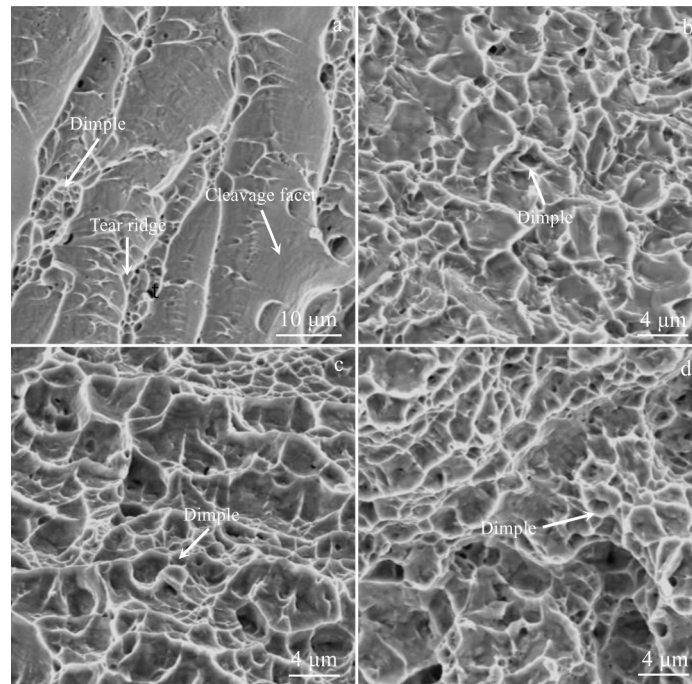


Fig.11 Influence of aging treatment on fracture morphology of joints: (a) as-welded joint, (b) 400 °C, (c) 500 °C, and (d) 600 °C

dislocations pile up at α/β interface, which significantly hinders dislocation motion and improves the strength.

The fracture surface morphologies of as-welded joints and heat-treated joints are displayed in Fig. 11. As depicted in Fig. 11a, dimples with relatively small size, cleavage facet, and tearing ridge are found on the surface, demonstrating

the quasi-cleavage fracture mode. After aging treatments at different temperatures for 8 h, numerous dimples are found on the fracture surface, as presented in Fig. 11b–11d, suggesting that the fracture mechanism is transformed from quasi-cleavage to microvoid coalescence fracture after the aging treatments.

The fracture surface is closely correlated with the microstructural characteristics. For the as-welded joints, because of the single β phase in fusion zone and near-HAZ, the fracture mode is consequence cleavage or quasi-cleavage fracture. Therefore, dimples, cleavage facet, and tearing ridge appear on the as-welded fracture surface. For the aged joints, there are many precipitates within β matrix. Due to the structure mismatch between precipitates and bcc β matrix, the ω/β and α/β interfaces will become the nucleating centers of microvoids during plastic deformation. As the deformation progresses, the microvoids coalescing eventually leads to the generation of dimples on the aged fracture surface.

4 Conclusions

1) For the as-welded Ti-3Al-6Mo-2Fe-2Zr (wt%) alloy joints, the high $[\text{Mo}]_{\text{eq}}$ and fast cooling rate result in the formation of single β phase microstructure in fusion zone as well as near-HAZ. In mid- and far-HAZ, α phase is partially retained due to the lower energy during laser welding.

2) The phase transformation in fusion zone changes from $\beta \rightarrow \omega \rightarrow \alpha$ to $\beta \rightarrow \alpha$ with increasing aging temperature. The size of α phase coarsens and the proportion of α phase decreases as aging temperature rises.

3) The tensile properties of the aged joints are evidently improved because of the second-phase strengthening of needle-shaped α phase. With increasing the aging temperature (from 400 °C to 600 °C), the coarsening of α phase and the reduction in volume fraction lead to the decrease in tensile

strength and the rise in elongation.

References

- 1 Semiatin S L. *Metallurgical and Materials Transactions A*[J], 2020, 51: 2593
- 2 Shariff T, Cao X, Chromik R R et al. *Canadian Metallurgical Quarterly*[J], 2011, 50(3): 263
- 3 Chamanfar A, Huang M F, Pasang T et al. *Journal of Materials Research and Technology*[J], 2020, 9(4): 7721
- 4 Sánchez-Amaya J M, Pasang T, Amaya-Vazquez M R et al. *Metals*[J], 2017, 7(7): 269
- 5 Lei Z L, Chen Y, Ma S C et al. *Materials Science and Engineering A*[J], 2020, 797: 140083
- 6 Long J, Zhang L J, Ning J et al. *Journal of Manufacturing Processes*[J], 2021, 64: 1329
- 7 Zhang Pingping, Wang Qingjuan, Gao Qi et al. *Hot Working Technology*[J], 2012, 41(14): 51 (in Chinese)
- 8 Wu C, Zhao Y Q, Huang S X et al. *Journal of Alloys and Compounds*[J], 2020, 841: 155728
- 9 Wang Q J, Wu J C. *Journal of Materials Engineering*[J], 2021, 49(9): 94
- 10 Zhang M Q, Li J S, Tang B et al. *International Journal of Plasticity*[J], 2022, 158: 103444
- 11 Wu X P, Zhang D Y, Guo Y W et al. *Journal of Alloys and Compounds*[J], 2021, 873: 159639

时效处理对 Ti-3Al-6Mo-2Fe-2Zr 激光焊接接头组织和性能的影响

万 轩, 何超威, 张可召, 刘 栋, 严春妍, 包晔峰
(河海大学 材料科学与工程学院, 江苏 常州 213022)

摘 要: 采用激光焊接近 β 钛合金 (Ti-3Al-6Mo-2Fe-2Zr), 并对激光焊接接头进行不同温度的时效处理, 揭示了时效温度、显微组织和接头拉伸性能之间的关系。结果表明, 由于该合金具有较高的 Mo 当量且激光焊接时冷却速度较快, 焊缝主要由单一 β 相组成。时效处理后, 在焊缝和热影响区中析出了大量的 α 相, 随着时效温度的升高, α 相粗化, 体积分数降低。与焊态接头相比, 时效处理后接头的抗拉伸强度和延伸率均有提升。但随时效温度的升高, α 相的体积分数减少, 强化效果减弱。当合金在 500 °C 时效 8 h 时, 接头获得了最佳的强度和塑性匹配。接头的断裂模式由焊态下的准解理断裂转变为时效处理后的微孔聚集型断裂。

关键词: β 钛合金; 激光焊接; 热处理; 显微组织演化; 室温拉伸性能

作者简介: 万 轩, 男, 2000年生, 硕士生, 河海大学材料科学与工程学院, 江苏 常州 213022, E-mail: 15779960828@163.com